AECL EACL

CA9600789

CA9600789

AECL-11440, COG-95-461

Anodic Dissolution of UO_2 in Slightly Alkaline Sodium Perchlorate Solutions

Dissolution anodique de l'UO_2 dans des solutions de perchlorate de sodium légèrement alcalines

S. Sunder, L.K. Strandlund, D.W. Shoesmith

April 1996 avril

VOL. 28 № 02

AECL EACL

ANODIC DISSOLUTION OF UO_2 IN SLIGHTLY ALKALINE SODIUM PERCHLORATE SOLUTIONS

by

S. Sunder, L.K. Strandlund and D.W. Shoesmith

Atomic Energy of Canada Limited
Whiteshell Laboratories
Pinawa, Manitoba, Canada R0E 1L0
1996

AECL-11440
COG-95-461

ANODIC DISSOLUTION OF UO_2 IN SLIGHTLY ALKALINE SODIUM PERCHLORATE SOLUTIONS

by

S. Sunder, L.K. Strandlund and D.W. Shoesmith

ABSTRACT

The anodic dissolution of UO_2 has been studied in aqueous sodium perchlorate solutions at pH ~ 9.5. Under potentiostatic conditions two distinct regions of oxidation/dissolution behaviour were observed. In the potential (E) range 0.100 V $\lesssim$ E $\lesssim$ 0.350 V (vs. SCE) currents decayed continuously with time due to the formation of oxidized surface films which gradually blocked further oxidation of the electrode. Steady-state currents were not achieved even after 24 hours. On the basis of anodic and cathodic charges (Q_A, Q_C respectively) obtained by integration of the anodic current-time plots (Q_A) and cathodic potential scans to reduce accumulated oxidized surface films (Q_C), it was shown that $\gtrsim$90% of the anodic oxidation current went to produce these films. For E $\gtrsim$ 0.350 V, steady-state currents were obtained and measurements of Q_A and Q_C showed the majority of the current went to produce soluble species.

The film blocking anodic dissolution appeared to be either $UO_{2.67}$ or, more probably, $UO_3 \cdot 2H_2O$ located primarily at grain boundaries. It is proposed that, at the higher potentials, rapid oxidation and dissolution followed by the hydrolysis of dissolved uranyl species leads to the development of acidic conditions in the grain boundaries. At these lower pH values the $UO_3 \cdot 2H_2O$ is soluble and therefore does not accumulate. Alternatively, if this oxide has been formed by prior oxidation at a lower potential, the formation of protons on oxidizing at E $\gtrsim$ 0.350V causes its redissolution, allowing the current to rise to a steady-state value. On the basis of Tafel slopes, an attempt was made to demonstrate that the observed behaviour was consistent with dissolution under acidic conditions. This analysis was only partially successful.

Atomic Energy of Canada Limited
Whiteshell Laboratories
Pinawa, Manitoba, Canada R0E 1L0
1996

AECL-11440
COG-95-461

DISSOLUTION ANODIQUE DE L'UO_2 DANS DES SOLUTIONS DE PERCHLORATE DE SODIUM LÉGÈREMENT ALCALINES

par

S. Sunder, L.K. Strandlund et D.W. Shoesmith

RÉSUMÉ

On a étudié la dissolution anodique de l'UO_2 dans des solutions aqueuses de perchlorate de sodium avec un pH d'environ 9,5. Dans des conditions potentiostatiques, on a observé deux régions distinctes de comportement d'oxydation et de dissolution. Dans la plage de potentiel (E), $0{,}100\ V \lesssim E \lesssim 0{,}350\ V$ (par rapport à une électrode au calomel standard), les courants se sont désintégrés continuellement avec le temps en raison de la formation de films superficiels oxydés qui ont enrayé graduellement toute oxydation supplémentaire de l'électrode. Les courants en régime permanent n'ont pas été atteints même après 24 heures. En se fondant sur les charges anodiques et cathodiques (respectivement Q_A et Q_c) obtenues par l'intégration des diagrammes courant-temps anodiques (Q_A) et des explorations du potentiel cathodique pour réduire les films de surface oxydés accumulés (Q_c), on a démontré que $\gtrsim$90 % ou plus du courant d'oxydation anodique produisait ces films. Pour $E \gtrsim 0{,}350$ V, on a obtenu des courants en régime permanent, et des mesures de Q_A et Q_c ont démontré que la majeure partie du courant produisait des espèces solubles.

Le film enrayant la dissolution anodique s'est révélé être soit l'$UO_{2,67}$ soit, plus probablement, l'$UO_3 \cdot 2H_2O$ situé principalement aux joints de grains. On propose que, à des potentiels plus élevés, l'oxydation et la dissolution rapides suivies de l'hydrolyse des espèces d'uranyle dissous entraînent le développement des conditions acides aux joints de grains. À ces faibles valeurs de pH, l'$UO_3 \cdot 2H_2O$ est soluble et par conséquent ne s'accumule pas. Par ailleurs, si cet oxyde a été formé par une oxydation antérieure à un potentiel inférieur, la formation de protons lors de l'oxydation à $E \gtrsim 0{,}350$ V entraîne sa redissolution, permettant au courant d'augmenter à une valeur de régime permanent. En se fondant sur les pentes de Tafel, on a tenté de démontrer que le comportement observé était compatible avec la dissolution dans des conditions acides. Cette analyse n'a été qu'un succès partiel.

Énergie atomique du Canada limitée
Laboratoires de Whiteshell
Pinawa (Manitoba) Canada R0E 1L0
1996

AECL-11440
COG-95-461

CONTENTS

		Page
1.	INTRODUCTION	1
2.	EXPERIMENTAL	2
	2.1 GENERAL	2
	2.2 PROCEDURE TO RECORD ANODIC OXIDATION/ *DISSOLUTION CURVES*	2
3.	RESULTS	3
4.	DISCUSSION	7
5.	SUMMARY AND CONCLUSIONS	14
	ACKNOWLEDGEMENTS	14
	REFERENCES	15
	FIGURES	19

1. INTRODUCTION

The assessment of the geological disposal of spent nuclear fuel requires a prediction of the dissolution rate of fuel as a function of disposal time. This dissolution rate is expected to be a function of redox conditions, since spent nuclear fuel is mainly UO_2 (>95%), a solid for which the solubility increases by many orders of magnitude under oxidizing conditions [1-20].

Redox conditions within a Canadian nuclear waste disposal vault will initially be oxidizing due to oxygen trapped in the buffer and backfill materials on sealing [1]. With time, conditions will evolve to nonoxidizing as this oxygen is consumed by corrosion of the container material and/or reaction with oxidizable minerals and organic impurities in the backfill. It is likely that this transitory oxidizing phase will not exceed the lifetime of the container. However, the possibility remains that the fuel will encounter oxidizing conditions on exposure to groundwater, due to the potential for production of oxidants by the radiolysis of water by gamma, beta and alpha radiation.

It has been shown that the dissolution (corrosion) of UO_2 is an electrochemical process which can be appropriately and conveniently studied by electrochemical methods [5-7, 15, 19-27]. Recently, we have published a simple electrochemical model to predict the dissolution rates of UO_2 as a function of the redox conditions prevailing in the solution environment to which the fuel is exposed [5, 6]. In this model the dissolution currents (i_D) measured on UO_2 electrodes as a function of applied electrochemical potential (E) are plotted as a Tafel plot (log i_D vs. E) and extrapolated to the steady-state corrosion potential ($(E_{CORR})_{SS}$) measured under natural corrosion conditions. The value of the corrosion current (i_{CORR}) obtained is the dissolution rate of UO_2 for the redox conditions prevailing in that particular solution. By measuring a series of values of $(E_{CORR})_{SS}$ in solutions of different redox conditions, the dissolution rate can be predicted as a function of the concentration of various oxidizing agents. In this manner, UO_2 dissolution rates have been predicted as a function of dissolved oxygen and hydrogen peroxide concentrations, and as a function of gamma and alpha radiation dose rates.

If reliable dissolution rates are to be predicted, the Tafel relationship must be known with confidence. Our previous predictions relied on a single set of dissolution current measurements (6 data points recorded on a single UO_2 specimen in 0.1 $mol \cdot L^{-1}$ $NaClO_4$ (pH = 9.5) [24]. Here, we describe the results of a more extensive series of measurements on a number of UO_2 specimens also performed in 0.1 $mol \cdot L^{-1}$ $NaClO_4$.

2. EXPERIMENTAL

2.1 GENERAL

UO_2 electrodes were constructed from pellets of sintered polycrystalline UO_2 taken from unused CANDU fuel elements. The design of the UO_2 electrode has been described previously [27]. The UO_2 disks used in preparing the electrodes were about 3 mm thick and about 1.4 cm in diameter. The geometric surface area was about 1.6 cm^2. The resistivity of the electrodes ranged between 5 and 10 $k\Omega \cdot cm$. The electrodes were polished using 600-grit SiC paper initially and before each series of step experiments. After polishing, the electrode was washed with pure water and reduced at -2.0 V vs. SCE (saturated calomel electrode) for 5 min in the electrochemical cell. The cell was of the standard three-electrode-three-compartment design and was purged with nitrogen. All potentials were measured and are quoted against this reference electrode. The electrolyte used was 0.1 $mol \cdot L^{-1}$ $NaClO_4$. The solution pH was adjusted using $HClO_4$. The $NaClO_4$, $HClO_4$, and NaOH were obtained from Aldrich, Mallinckrodt, and Fisher Scientific Company, respectively. Distilled water was further purified using a Millipore milli-R06+ unit (which includes separate cartridges to remove inorganic and organic impurities) followed by Milli-Q-Plus ion exchange columns. This procedure provided water with high purity as indicated by its high specific resistivity = 18.2 $M\Omega \cdot cm$.

Electrochemical data were obtained using a potentiostat/galvanostat (EG&G Princeton Applied Research model 273) controlled by a PC computer using a program PARC obtained from the manufacturer [28]. Data were recorded using an Electronic Controls Design Inc. model 50 data-logger. The angular velocity of the rotating-disc electrode was controlled by a Pine Instruments Model AFASR analytical rotator. Potentials were monitored using a Keithley 614 electrometer.

2.1 PROCEDURE TO RECORD ANODIC OXIDATION/DISSOLUTION CURVES

Figure 1 shows the potential time profiles used to record the anodic oxidation/dissolution currents on rotating disc electrodes. In all cases the electrode was polished and cathodically reduced at -2.0 V for ~5 min to remove any air-formed oxide films which may have been present on immersion of the electrode in the solution, as described above. Subsequently, two different procedures were used to record currents as a function of applied potential:

(1) The electrode was preoxidized at +0.100 V for various lengths of time between 1.5 h and 26 h (Figure 1). Then the potential was pulsed to a consecutive series of more positive potentials and the current recorded for up to 1.5 h at each potential before moving to the next (Figure 1). These potentials were in the range +0.100 to +0.500 V. In a small number of cases the currents were held for >1.5 h at certain potentials. Following the recording of current at the most positive potential, the potential was swept at a rate of 20 $mV \cdot s^{-1}$ from this anodic limit to -2.0 V and the current-potential relationship recorded.

(2) Alternatively, instead of preoxidizing the electrode at +0.100 V, the potential was pulsed directly from -2.0 V to a potential in the range +0.100 V to +0.500 V and the current recorded as a function of time (Figure 1). The potential was then swept back to -2.0 V and the current-potential relationship recorded. The electrode was then reprepared and cathodically reduced again at -2.0 V before repeating the procedure at a different potential in the range 0.100 V to 0.500 V.

3. RESULTS

Figure 2 shows logarithmic current (i) - time (t) plots recorded individually at a series of potentials without preoxidation at +0.100 V. At short times ($\log t \lesssim 0.1$), the current shows a similar dependence on time for all potentials although the absolute current increases with increasing potential. For $\log t \gtrsim 0.1$, the current decays with time over the duration of the experiment providing $E \lesssim 0.350$ V. This behaviour suggests oxidation of the UO_2 to produce films which eventually block the further oxidation of the electrode surface. The ability of these films to block further oxidation of the surface can be appreciated by the potentiostatic behaviour observed at +0.100 V over 26 h, Figure 3. After this time, the current has fallen to ~15 nA (~3 $nA \cdot cm^{-2}$ assuming a uniform distribution of current and an electrode surface area of ~4.8 cm^2 due to a roughness factor of ~3) and shows no apparent trend towards a steady-state value. This current represents a lower limit below which a meaningful value is unobtainable. For $E \gtrsim 0.350$ V, the current achieves a steady-state value, indicating that oxidation of the surface does not lead to its blockage, Figure 2. The potential range over which this transition from decaying to steady-state currents occurs is not particularly well-defined, and variability in behaviour is often observed in the range $0.300 \text{ V} < E < 0.400$ V.

Figure 4 shows a similar series of logarithmic i-t plots recorded consecutively at a sequence of potentials after preoxidation at +0.100 V for ~24 h. Again, for $E \lesssim 0.350$ V, the current

decays continuously with time over the 1.5 h period for which the potential is held at each value in the sequence. The currents at short times are almost an order of magnitude lower than in the absence of preoxidation due to the partial blockage of the oxidation process by film growth at the preoxidation potential of +0.100 V. At higher potentials (+0.450 V in Figure 4, but generally at any potential >0.350 V) the current increases with time finally achieving a steady-state value (i_{ss}) after ~1.5 h. This increase suggests the oxidized surface films which grow and block oxidation at lower potentials are subsequently removed at higher potentials. The oxidized layer remaining on the surface at high potentials, is essentially ineffective in blocking the oxidation of UO_2, Figures 3 and 4 (vide-infra).

The presence of surface oxide films is confirmed by the i-E relationships recorded when the potential is scanned from the anodic limit to -2.0 V, Figure 5. These scans were recorded after completion of the anodic oxidations for which the log i-log t plots are shown in Figure 2. Three reduction peaks (1 (-0.670 to -0.750 V), 2 (-0.830 to -0.870 V) and 3 (-0.120 V)) are observed and, as demonstrated previously [19,27], can be attributed to the reduction of oxide films formed on the UO_2 surface during anodic oxidation. Peak 1 is ubiquitously present no matter what the oxidation potential. Peak 2 is present after oxidation at 0.175 V and increases in size as the anodic potential is increased up to ~+0.350 V. In fact, peak 2 is present after oxidation at potentials as low as +0.100 V. It would appear that the growth of this oxide is the cause of the current decay (Figures 3 and 4). After oxidation at anodic limits >0.350 V peak 2 is either much smaller or absent altogether (D,E in Figure 5). The behaviour of the minor peak 3 is difficult to determine but appears to be very similar to that of peak 2.

The charge consumed in reducing these oxidized surface films, Q_C, can be determined by integrating the area under the reduction peaks in Figure 5 as indicated by the shaded area for the i-E profile recorded after 1.5 h of anodic oxidation at +0.175 V. Figure 6 shows a plot of the charge ratio Q_C/Q_A as a function of the applied anodic potential (E_A) for many such experiments. All the data in this plot are from experiments in which the oxidation was performed potentiostatically at a single potential. The total charge, Q_A, is that consumed by anodic oxidation at this single potential (E_A).

For oxidation at potentials $\lesssim$0.300 V the Q_C/Q_A charge ratio is ~0.9, an indication that the majority of the charge consumed during anodic oxidation is recovered during the cathodic reduction of the surface oxidized films. (The single value of $Q_C/Q_A > 1$ (at 0.260 V) suggests a value of Q_C influenced by the reduction of residual traces of oxygen in the solution.) Thus, in this potential range, in which currents decay logarithmically with time (Figure 2), oxidation leads predominantly to the formation of surface films. The small fraction, 0.1, of the anodic

charge unaccounted for by the subsequent film reduction process could be lost by dissolution (as U^{VI}). Alternatively, its loss could be attributable to the <100% efficiency of the cathodic oxide reduction process. Analysis of the reduced surface by X-ray photoelectron spectroscopy shows that its composition is ~$UO_{2.1}$, and photoelectrochemical studies confirm that the oxidation is totally irreversible [19].

For E > 0.300 V, the ratio Q_C/Q_A decreases markedly, mainly due to an increase in the value of Q_A. Values of ~0.2 are achieved for $E \gtrsim 0.400$ V and, for E = 0.500 V, the ratio is effectively zero. Since little of the anodic charge is recovered during the cathodic reduction sweep it can be considered consumed to produce dissolved U^{VI} species which are lost by transport to the bulk of the solution. This occurs in the potential region where steady-state currents are observed, Figures 2 and 4, which can, therefore, be attributed to oxidative dissolution.

The final values of the currents recorded over the whole potential range (+0.100 V to +0.500 V) are plotted logarithmically as a function of applied potential in Figure 7. On the basis of the evidence presented above, the plot can be divided into two distinct regions: a region, for $E \lesssim 0.350$ V when oxidized films build up and block the electrode surface, and a region, for $E \gtrsim 0.350$ V, when steady-state dissolution predominates. The two major sets of data points (▲, ○) show currents obtained on two UO_2 electrodes cut from different UO_2 fuel pellets. The columns of data points at +0.100, +0.200 and +0.300 V show the effects of prolonged potentiostatic oxidation at these potentials. The larger currents were obtained after oxidation for 1.5 h whereas the lower currents were obtained after progressively longer periods of oxidation. The lowest current plotted for +0.100 V was recorded after 26 h of oxidation, Figure 3, and the lowest points at +0.200 V and +0.300 V were recorded after ~24 h. Even for these durations, the currents had shown no tendency to achieve steady-state, confirming that a steadily increasing blockage of the oxidation process by film formation was occurring. Although the results are not included in Figure 7, some experiments were also performed with stationary electrodes. The effect of electrode rotation rate on the oxidation current was minor demonstrating that the formation of oxide films was not prevented by the transport of dissolved uranyl species away from the electrode surface. Clearly, a simple dissolution/ precipitation process cannot be invoked to explain film formation. If anything, there is some evidence that the currents in the transition region between non steady-state and steady-state behaviour (0.300 V to 0.400 V) are slightly higher at stationary electrodes.

For E > 0.350 V, the currents increase with potential, but are quite scattered. The extent of the scatter can be appreciated from the points plotted for 0.400 V, which range over nearly two orders of magnitude. Despite this scatter, a linear fit to these data (for E > 0.300 V)

yielded a Tafel slope of 58 ± 5 mV^{-1} (thick line in Figure 7). This is close to the 62.5 mV^{-1} obtained with our previously published data [15] shown as the thin line in Figure 7. If we fit the data points for the two different electrodes independently then Tafel slopes of 62 ± 8 mV^{-1} (▲, Figure 8A) and 54 ± 4 mV^{-1} (O, Figure 8B) are obtained for electrodes L and R respectively. Closer inspection of the data points obtained with electrode R suggests a fit to two distinct linear regions, 0.350 V ≤ E ≤ 0.400 V and 0.400 V ≤ E ≤ 0.550 V, may be more appropriate. When the data for electrode R are fitted in this manner, Tafel slopes of 31.3 ± 3.7 mV^{-1} and 109 ± 22 mV^{-1} are obtained, Figure 8C.

A similar scatter is also apparent in the values of Q_A and Q_C which are plotted as a function of E_A, the single potential at which the oxidation was performed, in Figure 9. The lines in this figure are crude envelopes for the values of Q_A and Q_C and serve only to indicate the trends. Around ~0.350 V, Q_A begins to increase markedly, reflecting the differences in i-t behaviour observed above and below this potential, Figures 2 and 4. The ranges of Q_A and Q_C values are wide, especially in the potential range 0.350 V $\lesssim$ E $\lesssim$ 450 V. Within this potential range, low values of Q_C are inevitably recorded in experiments for which high values of Q_A are obtained and vice versa. Thus, a significant amount of scatter in the dissolution currents in the steady-state region of Figure 7 can be attributed to the irreproducibility of the balance between oxidative film formation on, and oxidative dissolution of, the UO_2 electrode surface.

Figure 10 shows plots of i_{ss} and Q_A as functions of the final pH of the solution. In this figure Q_A is the total charge consumed either by anodic oxidation at a single potential, $E_A > 0.350$ V, or at a sequence of potentials culminating in a final oxidation at E_A, and i_{ss} is the final steady-state dissolution current achieved at E_A and plotted in Figure 7. Clearly, the higher the anodic dissolution current (i_{ss}) and the larger the total extent of oxidation (Q_A), the lower is the final pH of the solution due to the hydrolysis of dissolved uranyl species.

Figure 11 shows a series of voltammograms recorded on the same UO_2 electrode (R) after various treatments. The first scan was recorded on a freshly polished electrode from -2.000 V to +0.300 V and back again. The second scan was performed from the final potential to -2.000 V and back after the electrode had been preoxidized at +0.100 V for 16 h and then oxidized at a sequence of potentials for 1.5 h each up to a final potential of 0.440 V. The third scan was performed, again from the final potential to -2.000 V and back, after a similar pretreatment and sequence of oxidations up to a final potential of 0.500 V. The differences to note between the pretreatment before the second and third voltammograms are the final steady-state currents (158 μA and 261 μA, respectively), and the total amounts of anodic

charge (211 mC and 2550 mC, respectively). This large difference was due predominantly to the 1.5 h of oxidation at 0.500 V prior to the third voltammogram.

4. DISCUSSION

We have shown previously that the surface chemistry of UO_2 is complex in the potential region investigated here (+0.100 to +0.500 V) [19,26,27]. The results presented in this report demonstrate that the surface chemistry has a major influence on the oxidative dissolution process. Using a combination of electrochemical and XPS techniques, we assigned peak 1 in Figure 5 to the reduction of $UO_{2.33}$ to UO_{2+x}, peak 2 to the reduction of $UO_{2.67}$ to UO_{2+x} and peak 3 to the reduction of $UO_3 \cdot 2H_2O$ to UO_{2+x} [19,27].

The occurrence of peak 3 at a potential as positive as ~-0.2 V indicates this species is easily reduced, and assignment of this peak to the reduction of a secondary phase formed by a solution-mediated recrystallization ($UO_3 \cdot 2H_2O$) seems less certain [27]. To account for the fact that only a very small charge (Q_C) was associated with the reduction of this film, irrespective of whether it was formed electrochemically or by natural corrosion, we postulated that it was only present in small quantities in grain boundaries. This suggests that both electrochemical and corrosion reactions are concentrated at grain boundary sites.

Despite the small amount of charge involved, this layer, when present as a consequence of natural corrosion, supports higher currents for the electrochemical reduction of oxygen than those measured when it is absent. This is not consistent with its being an insulating layer. The reduction of oxygen on UO_2 electrodes appears to involve the utilization of donor-acceptor sites on the electrode surface [29,30]. This requires that adjacent uranium cations be in different oxidation states. The optimum configuration would be a surface monolayer containing U^{VI} cations with adjacent U cations in a lower oxidation state (i.e., U^{V} or U^{IV}). The presence of such a monolayer would be consistent with our claim that a layer containing U^{VI} species exists on the electrode surface and can act as a precursor to either the formation of oxide films or dissolved uranyl species [27]. In our earlier papers we designated this as an adsorbed UO_2^{2+} layer. While its actual chemical identity may remain in doubt, the results presented here are consistent with its existence as a precursor to film formation/dissolution. Whether or not it exists only at grain boundaries has not been determined.

The assignment of peak 1 (Figure 5) to the reduction of a $UO_{2.33}$ layer is consistent with all our previous observations under both electrochemical and natural corrosion conditions. A

layer close in stoichiometry to $UO_{2.33}$ has been shown to form by oxidation of the UO_2 lattice at potentials as low as -0.100 V, [31].

$$UO_2 + 0.33H_2O \rightarrow UO_{2.33} + 0.66H^+ + 0.66e \quad (1)$$

The present results show that such a layer remains on the electrode surface even after steady-state anodic dissolution for extended periods of time at positive potentials >0.350 V, E in Figure 5.

It is the film reduced at peak 2 (Figure 5) which appears to account for the current decay observed for $E \lesssim 0.350$ V. The size of this peak increases with increasing potential, or with the duration of oxidation at a single potential, in the low potential region, but decreases and eventually disappears under the steady-state dissolution conditions which prevail at higher potentials, Figure 7. Even when a substantial layer of this oxide is grown at $E \lesssim 0.350$ V, subsequent potentiostatic oxidation at higher potentials leads to its removal and an increase in the current until steady-state dissolution conditions are eventually achieved, Figure 4.

We have shown that anodically grown oxide films suppress the cathodic reduction of oxygen (at $E \lesssim -0.300$ V) [29,30]. While a direct correlation between this suppression and the presence of the oxide reduced at peak 2 (Figure 5) remains to be established, it is clear that this oxide possesses insulating properties. Previously, we have attributed peak 2 to the reduction of a layer of $UO_{2.67}$. If that is the case, its removal at more positive potentials (+0.400 V in Figure 4) could be attributed to the oxidative dissolution of this phase to produce dissolved UO_2^{2+}. However, this phase is unstable with respect to $UO_3 \cdot 2H_2O$ at a potential of ~-0.200 V [15-19]. Since $UO_{2.67}$ is not an insulator [19] it would not be expected to block the oxidation of UO_2 by requiring an overpotential of >0.550 V for its oxidative dissolution.

An alternative possibility is that peak 2 is due to the reduction of a layer of $UO_3 \cdot 2H_2O$ which does possess insulating properties. From the charges associated with the reductions at peaks 1 and 2 (Figure 5) after oxidation in the potential range 0.350 V to 0.400 V, we can estimate that, if evenly distributed across the electrode surface, these oxide films would be ~20 to 30 nm thick. Since peak 2 requires approximately one half of this charge, the $UO_3 \cdot 2H_2O$ would be 10-15 nm thick. This is extremely thin for an insulating layer formed by a solution-mediated recrystallization. Such layers would be expected to be somewhat porous and to require growth to much greater thicknesses in order to block the electrode surface. Also, if formed uniformly across the electrode surface in this manner, we would expect the thickness

of this oxide to be sensitive to the angular rotation rate of the disc electrode. This is not observed, the dependence of current on electrode rotation rate being very small.

All this evidence suggests that the $UO_3 \cdot 2H_2O$ could be located at grain boundaries. Then the insensitivity to hydrodynamic conditions would not be surprising and relatively small amounts of "higher" oxide could produce quite deep insulating deposits that would constitute a relatively small fraction of the total surface area of the electrode. The formation and removal of this oxide film would then depend on the local chemical conditions in the grain boundaries. Scanning electron microscopic examination of electrodes subjected to extensive electrochemical oxidation showed extensive attack at grain boundaries [32].

In an electrochemical, as opposed to natural corrosion experiment, the anode and cathode are separated on different electrodes in separate compartments of the cell. Consequently, there is the possibility that local excursions in chemical conditions, especially in pH, could exist at the working electrode, in this case, the UO_2 electrode. The incorporation of O^{2-} into surface films during film growth ($UO_2 \rightarrow UO_{2+x}$) and the production of hydrolyzable UO_2^{2+} species due to dissolution will both lead to the production of protons. Under natural corrosion conditions *this will be, at least partially, neutralized by the production of hydroxyl ions due to* O_2 reduction

$$O_2 + 2H_2O + 4e^- \rightarrow 4OH^- \qquad (2)$$

at adjacent sites on the same surface. Under electrochemical conditions the buildup of local acidity will not be neutralized, and if occurring predominantly in grain boundaries, will not necessarily be prevented by rotation of the electrode. While the data plotted in Figure 10 clearly show that extensive anodic dissolution does lead to a decrease in pH, it does not confirm that the process is predominantly localized in grain boundaries.

We can summarize the electrochemical oxidation/dissolution of UO_2 in the following mechanism. Oxidation of the $UO_{2.33}$ layer leads to the formation of an intermediate U^{VI} species,

$$UO_{2.33} + 0.33H_2O \rightarrow (UO_2^{2+})_{ads} + 0.66OH^- + 1.34e \qquad (3)$$

This intermediate may subsequently dissolve or become incorporated into oxidized surface phases,

$$3UO_{2.33} + 3(UO_2^{2+})_{ads} + 3H_2O \rightarrow 6UO_{2.67} + 6H^+ \quad (4)$$

$$(UO_2^{2+})_{ads} + 3H_2O \rightarrow UO_3{\cdot}2H_2O + 2H^+ \quad (5)$$

Of these two options (i.e., reactions (4) or (5)) the formation of $UO_3{\cdot}2H_2O$ by the hydrolysis of $(UO_2^{2+})_{ads}$ appears the kinetically more feasible reaction.

In the low potential region ($E \lesssim 0.350$ V) in which film growth predominates, the development of acidity by the occurrence of reactions (4) and (5) in grain boundaries does not appear to be sufficient to increase the solubility of U^{VI} species and prevent their incorporation into oxidized surface phases which eventually block reaction (3). At higher potentials ($E \gtrsim 0.350$ V) the production of uranyl species (UO_2^{2+}) is rapid and dissolution more extensive. The rapid and extensive hydrolysis of these uranyl species

$$2UO_2^{2+} + 2H_2O \rightarrow (UO_2)_2(OH)_2^{2+} + 2H^+ \quad (6)$$

$$3UO_2^{2+} + 5H_2O \rightarrow (UO_2)_3(OH)_5^{+} + 5H^+ \quad (7)$$

could lead to the development of low pH at the oxidation sites in the grain boundaries. The solubility of $UO_3{\cdot}2H_2O$ increases markedly below pH ~ 5.5 [15-19] and its formation could thus be prevented. This would leave the oxidation sites unblocked by the presence of oxidized phases and free to dissolve at a current dictated by the applied potential. The large variations in dissolution current values (Figure 7) and in Q_C values (Figure 9) for the same anodic treatment of the electrode indicates that the conditions in the grain boundaries are widely variable, and not necessarily reproducible, from one specimen of UO_2 to the next. It is clear from the steady-state dissolution currents plotted in Figure 7 that, although the dissolution mechanism may remain unchanged, no single simple equation precisely describes the relationship between potential and dissolution current for all UO_2 specimens.

The surface remaining after extensive anodic dissolution is much more reactive with respect to reoxidation, Figure 11. At present, the origin of this increased reactivity is not known but it increases with the extent of anodic dissolution (as measured by Q_A). An increase in extent and rate of oxidation has been observed with highly non-stoichiometric specimens ($\gtrsim UO_{2.1}$) [32] and it is possible that for more extensive and/or aggressive anodic treatments a partial oxidation of the surface (to UO_{2+x} with $x < 0.33$) occurs to a substantial depth into the electrode. Alternatively, roughening of the electrode due to extensive oxidative dissolution could lead to a much greater available surface area for the subsequent reoxidation process. This would account for the much larger oxidation currents in the anodic portions of the

voltammetric sweeps in Figure 11. The decay in current after the oxidation peak could then be explained by the rapid accummulation of $UO_3 \cdot 2H_2O$ deep in the grain boundaries of the oxide. For this to be the case the reactivity of the grain boundaries with respect to electrochemical oxidation and dissolution must be very much greater than that of the residual grains. That this is the case appears to be borne out by the SEM examinations of electrodes subjected to extensive electrochemical oxidation [32].

Previously, Nicol and Needes proposed the following mechanism for the anodic dissolution of UO_2 [22],

$$UO_2 + H_2O \rightarrow UO_2OH + H^+ + e^- \quad (8)$$

$$UO_2OH \rightarrow UO_3 + H^+ + e^- \quad (9)$$

$$UO_3 + 2H^+ \rightarrow UO_2^{2+} + H_2O \quad (10)$$

While different in format, this mechanism has close similarities to the one presented in this report. While we have not specifically proposed a U^V intermediate, the thin $UO_{2.33}$ layer (~5 to 8 nm [27]) can be thought of as a surface layer in which the uranium species are in the oxidation states IV and V with two U^V species for each U^{IV}. The UO_3 layer proposed by Nicol and Needes as an intermediate in the dissolution process is similar in concept to the U^{VI} intermediate we claim as reduced at peak 3, Figure 5.

Given these similarities, the kinetic scheme of Nicol and Needes can be adapted in an attempt to describe our results for dissolution under steady-state conditions ($E \gtrsim 0.350$ V). In acidic solutions, equivalent to those proposed to exist in grain boundaries, the dissolution of UO_3 will be rapid compared to its rate of production and coverage of the surface by the UO_3 intermediate will be negligible. The dissolution current is then given by

$$i_D = 2Fk_2\theta\exp\left\{(1-\beta_2)\frac{EF}{RT}\right\} \quad (11)$$

where θ is defined by Nicol and Needes [33] as the fractional surface coverage by UO_2OH, k_2 is the rate constant and β the symmetry factor for reaction (9). According to our reaction scheme, it is more appropriate to view θ as a variation in stoichiometry of the $UO_{2.33}$ with applied potential. Some experimental evidence exists to support this view [31].

Under steady-state conditions the rate of formation of U^v (or the $UO_{2.33}$ layer) is given by

$$v_1 = k_1 (1-\theta)\exp\left\{(1-\beta_1)\frac{EF}{RT}\right\} \tag{12}$$

and its rate of disappearance by

$$v_2 = k_2\theta\exp\left\{(1-\beta_2)\frac{EF}{RT}\right\} + k_{-1}[H^+]\theta\exp\left\{-\beta_1\frac{EF}{RT}\right\} \tag{13}$$

where k_1, k_{-1} are the rate constants for reaction (8) which is taken to be reversible and β_1 is the symmetry factor for this reaction.

Eliminating θ by substitution in Equation (11) yields

$$i_D = 2Fk_1k_2\exp\left\{(1-\beta_1)\frac{EF}{RT}\right\}\exp\left\{(1-\beta_2)\frac{EF}{RT}\right\}\bullet A^{-1} \tag{14}$$

where A is given by

$$A = k_1\exp\left\{(1-\beta_1)\frac{EF}{RT}\right\} + k_2\exp\left\{(1-\beta_2)\frac{EF}{RT}\right\} + k_{-1}[H^+]\exp\left\{-\beta_1\frac{EF}{RT}\right\} \tag{15}$$

Two possible approximations exist.

(a) For low anodic potentials

$$k_{-1} \gg k_1, k_2$$

and only the third term in A will be significant. The dissolution current is then given by

$$i_D = 2Fk_1k_2(k_{-1})^{-1}[H^+]^{-1}\exp\left\{(2-\beta_2)\frac{EF}{RT}\right\} \tag{16}$$

which predicts a Tafel slope of 40 mV^{-1} if it is assumed that $\beta_2 = 0.5$. It also predicts an inverse acid dependence with a cathodic shift of 40 mV^{-1} for each unit increase in pH. This equation does describe both the Tafel and pH behaviour observed by Nicol and Needes for pH $\lesssim$ 2, but the Tafel slope is inconsistent with our observation (58 ± 5 mV^{-1}).

(b) For high anodic potentials

$$k_{-1} \ll k_1, k_2$$

and the last term in A can be neglected yielding for i_D the expression

$$i_D = 2Fk_1k_2(k_1+k_2)^{-1}\exp\left\{(1-\beta)\frac{EF}{RT}\right\} \qquad (17)$$

providing it is assumed $\beta_1 = \beta_2 = \beta$. This expression predicts no dependence on pH and a Tafel slope of 120 mV^{-1}, a value which is again inconsistent with our observations.

For pH values around 9, Nicol and Needes obtained Tafel slopes 70 and 80 mV^{-1} in sodium perchlorate solutions. Our values for the two different UO_2 electrodes 54 ± 4 mV^{-1} and 62 ± 8 mV^{-1} are closer to the values they obtained in sodium sulphate solutions. They noted that slopes close to 60 mV^{-1} suggested a single two electron transfer was involved but placed little faith in such a conclusion. For the L electrode a fit to two Tafel slopes, 31 ± 4 mV^{-1} at low potentials and 109 ± 22 mV^{-1} at higher potentials, could be obtained, consistent with the two limiting kinetic cases for acidic solutions (pH $\lesssim$ 2) expressed by equations (16) and (17). However, given the scatter in the data, such a fit must be considered tentative at best, and we cannot unequivocally conclude that the dissolution reaction occurs in two kinetically distinguishable one electron transfer steps as expected in acidic solutions. An equally feasible explanation for the decreased dependency of dissolution current on potential observed for electrode L at high potentials (Figure 8C) is the reaccumulation of precipitated $UO_3 \cdot 2H_2O$. For the high anodic dissolution currents achieved, the rate of local production of UO_2^{2+} species in grain boundaries may be sufficient to exceed the solubility product despite the accompanying local acidification.

5. SUMMARY AND CONCLUSIONS

The anodic oxidation and dissolution of UO_2 in neutral and slightly basic solutions can be divided into two distinct regions of behaviour.

1. For $0.100\ V \leq E \lesssim 0.350\ V$ the electrode becomes covered with oxidized surface films which block the further oxidation of the electrode. The electrode is covered by a thin (5 to 8 nm) layer of $UO_{2.33}$ and a deposited film of $UO_{2.67}$ or, more probably, $UO_3 \cdot 2H_2O$ which appears to be located predominantly at grain boundaries.

2. For $E \gtrsim 0.350\ V$ the electrode undergoes steady-state dissolution and the dissolution currents obey a Tafel relationship, although they vary from one electrode to another. Dissolution appears to be concentrated at grain boundaries. Hydrolysis of the uranyl dissolution product leads to local acidification at these sites. This drop in pH either prevents the formation of the oxidized surface layer which blocks oxidation and dissolution at lower potentials or causes its redissolution if it has been preformed at lower potential.

The Tafel slope of $58 \pm 5\ mV^{-1}$ suggests a single two electron transfer is involved but this seems highly improbable. There is some evidence with one electrode that dissolution under steady-state conditions may occur in two kinetically distinguishable one electron transfer steps as expected for acidic conditions. However, given the scatter in the data, this evidence must be considered inconclusive

ACKNOWLEDGEMENTS

We are grateful to W.H. Hocking and S. Stroes-Gascoyne for helpful comments on the manuscript. This work is part of the Canadian Nuclear Fuel Waste Management Program which is jointly funded by AECL and Ontario Hydro under the auspices of the CANDU Owners Group.

REFERENCES

1. Johnson, L.H., D.M. Leneveu, D.W. Shoesmith, D.W. Oscarson, M.N. Gray, R.J. Lemire and N.C. Garisto. 1994. The disposal of Canada's Nuclear Fuel Waste: The Vault Model for Postclosure Assessment, Atomic Energy of Canada Limited Report, AECL-10714, COG-93-4.

2. Grambow, B., A. Loida, P. Dressler, H. Geckeis, P. Diaz, J. Gago, I. Casas, J. de Pablo, J. Gimenes and M.E. Torrero. 1994. Long-term safety of radioactive waste disposal: reaction of high burnup spent fuel and UO_2 in saline brines at room temperature, Kernforschungszentrum, Karlsruhe, KfK 5377.

3. Forsyth, R.S. and L.O. Werme. 1992. Spent fuel corrosion and dissolution. J. Nucl. Mater., 190, 3-19.

4. Gray, W.J., H.R. Leider and S.A. Steward. 1992. Parametric study of LWR spent fuel dissolution kinetics. J. Nucl. Mater., 190, 46-52.

5. Shoesmith, D.W. and S. Sunder. 1992. The prediction of nuclear fuel (UO_2) dissolution rates under waste disposal conditions. J. Nucl. Mater., 190, 20-35. Also Atomic Energy of Canada Limited Reprint, AECL-10677.

6. Shoesmith, D.W. and S. Sunder. 1991. An electrochemistry-based model for the dissolution of UO_2. Atomic Energy of Canada Limited Report, AECL-10488.

7. Sunder, S. and D.W. Shoesmith. 1991. Chemistry of UO_2 fuel dissolution in relation to the disposal of used nuclear fuel. Atomic Energy of Canada Limited Report, AECL-10395.

8. Parks, G.A. and D.C. Pohl. 1988. Hydrothermal solubility of uraninite. Geochim. Cosmochim. Acta, 52, 863-875.

9. Lemire, R.J. and F. Garisto. 1989. The solubility of U, Nb, Pu, The and Tc in a geological disposal vault for used nuclear fuel. Atomic Energy of Canada Limited Report, AECL-10009.

10. Bruno, J., I. Casas and I. Puigdomènech. 1988. The kinetics of dissolution of UO_2 (s) under reducing conditions. Radiochimica Acta, 44/45, 11-16.

11. Bruno, J., I. Casas and I. Puigdomènech. 1991. The kinetics of dissolution of UO_2 under reducing conditions and the influence of an oxidized surface layer (UO_{2+x}): Application of a continuous flow-through reactor. Geochimica et Cosmochimica Acta 55, 647-658.

12. Johnson, L.H. and D.W. Shoesmith. 1988. Spent fuel, In Radioactive Waste Forms for the Future (W. Lutze and R.C. Ewing, eds), Elsevier Publishers Science Publishers B.V. 635-698. Also Atomic Energy of Canada Limited Reprint, AECL-9583.

13. Garisto, F. and N.C. Garisto. 1985. A UO_2 solubility function for the assessment of used nuclear fuel disposal. Nuclear Science and Engineering 90, 103-110. Also Atomic Energy of Canada Limited Reprint, AECL-8515.

14. Christensen, H., S. Sunder, and D.W. Shoesmith. 1994. Development of a kinetic model to predict the rate of oxidation and dissolution of nuclear fuel (UO_2) by the radiolysis of water. Atomic Energy of Canada Limited Report, AECL-11102, COG-93-488.

15. Sunder, S., D.W. Shoesmith, R.J. Lemire, M.G. Bailey and G.J. Wallace. 1991. The effect of pH on the corrosion of nuclear fuel (UO_2) in oxygenated solutions. Corrosion Science 32, 373-386. Also Atomic Energy of Canada Limited Reprint, AECL-10093.

16. Lemire, R.J. and P.R. Tremaine. 1980. Uranium and plutonium equilibria in aqueous solutions to 200°C. Journal of Chemical Engineering Data 25, 361-370. Also Atomic Energy of Canada Limited Reprint, AECL-6655.

17. Paquette, J. and R.J. Lemire. 1981. A description of the chemistry of aqueous solutions of uranium and plutonium at 200°C using potential-pH diagrams. Nuclear Science and Engineering 79, 26-48. Also Atomic Energy of Canada Limited Reprint, AECL-7037.

18. Grenthe, I., J. Fuger, R.J.M. Konings, R.J. Lemire, A.B. Muller, C. Nguyen-Trung and H. Wanner, "Chemical Thermodynamics of Uranium, Volume 1, Chemical Thermodynamics," H. Wanner and I. Forest, editors, North Holland, Amsterdam (1992).

19. Shoesmith, D.W., S. Sunder and W.H. Hocking. 1994. Electrochemistry of UO_2 nuclear fuel. In Electrochemistry of Novel Materials (editors, J. Lipkowski and P.N. Ross) VCH Publishers Inc., New York, 297-337.

20. Grambow, B. 1989. Used fuel dissolution and oxidation. An evaluation of literature data. SKB Technical Report, SKB 89-13.

21. Needes, C.R.S., M.J. Nicol and N.P. Finkelstein. 1975. Electrochemical model for the leaching of uranium dioxide: 2 - Alkaline carbonate media. In Leaching and Reduction in Hydrometallurgy (A.R. Burkin, editor). Inst. Min. Metall., London, U.K., 12-19.

22. Nicol, M.J. and C.R.S. Needes. 1975. The anodic dissolution of uranium dioxide - 1. In perchlorate solutions. Electrochimica Acta 20, 585-589.

23. Nicol, M.J., C.R.S. Needes and N.P. Finkelstein. 1975. Electrochemical model for the leaching of uranium dioxide: 1 - Acid media. In Leaching and Reduction in Hydrometallurgy (A.R. Burkin, editor). Inst. Min. Metall., London, U.K., 1-11.

24. Shoesmith, D.W., S. Sunder, M.G. Bailey and G.J. Wallace. 1989. The corrosion of nuclear fuel (UO_2) in oxygenated solutions. Corros. Sci. 29, 1115-1128. Also Atomic Energy of Canada Limited Reprint, AECL-9887

25. Rudnicki, J.D., R.E. Russo and D.W. Shoesmith. 1994. Photothermal deflection spectroscopy investigations of uranium dioxide oxidation. J. Electroanal. Chem. 372, 63-74.

26. Shoesmith, D.W., W.H. Hocking, S. Sunder, J.S. Betteridge and N.H. Miller. 1994. electrochemical studies of SIMFUELs. J. Alloys and Comps. 213/214, 551-553. Also Atomic Energy of Canada Limited Reprint, AECL-11086, COG-94-200.

27. Sunder, S., D.W. Shoesmith, M.G. Bailey, F.W. Stanchell and N.S. McIntyre. 1981. Anodic oxidation of UO_2 - Part 1. Electrochemical and X-Ray photoelectron spectroscopic studies in neutral solutions. J. Electroanal. Chem. 130, 163-179. Also Atomic Energy of Canada Limited Reprint, AECL-7139.

28. EG&G PARC. 1989. Softcore corrosion measurement. Software operating manual.

29. Hocking, W.H., J.S. Betteridge and D.W. Shoesmith. 1991. The cathodic reduction of dioxygen on uranium oxide in dilute alkaline aqueous solution. Atomic Energy of Canada Limited Report, AECL-10402.

30. Hocking, W.H., J.S. Betteridge and D.W. Shoesmith. 1994. The cathodic reduction of oxygen on uranium dioxide in dilute alkaline aqueous solution. J. Electroanal. Chem. 379, 339-351. Also Atomic Energy of Canada Limited Reprint, AECL-11433.

31. Sunder, S., D.W. Shoesmith, N.H. Miller and G.J. Wallace. 1992. Determination of criteria for selecting a UO_2 dissolution model for the nuclear fuel waste management concept assessment. Mater. Res. Soc. Symp. Proc. 257, 345-352. Also Atomic Energy of Canada Limited Reprint, AECL-10532.

32. Johnson, L.H., D.W. Shoesmith, G.E. Lunansky, M.G. Bailey and P.R. Tremaine. 1982. The mechanisms of leaching and dissolution of uranium oxide fuel. Nuclear Technology 26, 238-253. Also Atomic Energy of Canada Limited Reprint, AECL-6992.

33. Hocking, W.H., S. Sunder, J.S. Betteridge and D.W. Shoesmith. Unpublished results.

34. Nicol, M.J. and C.R.S. Needes. 1973. The mechanism of the anodic dissolution of Uranium Dioxide. Nat. Inst. Met. Repub. S. Africa, Report No. 7079.

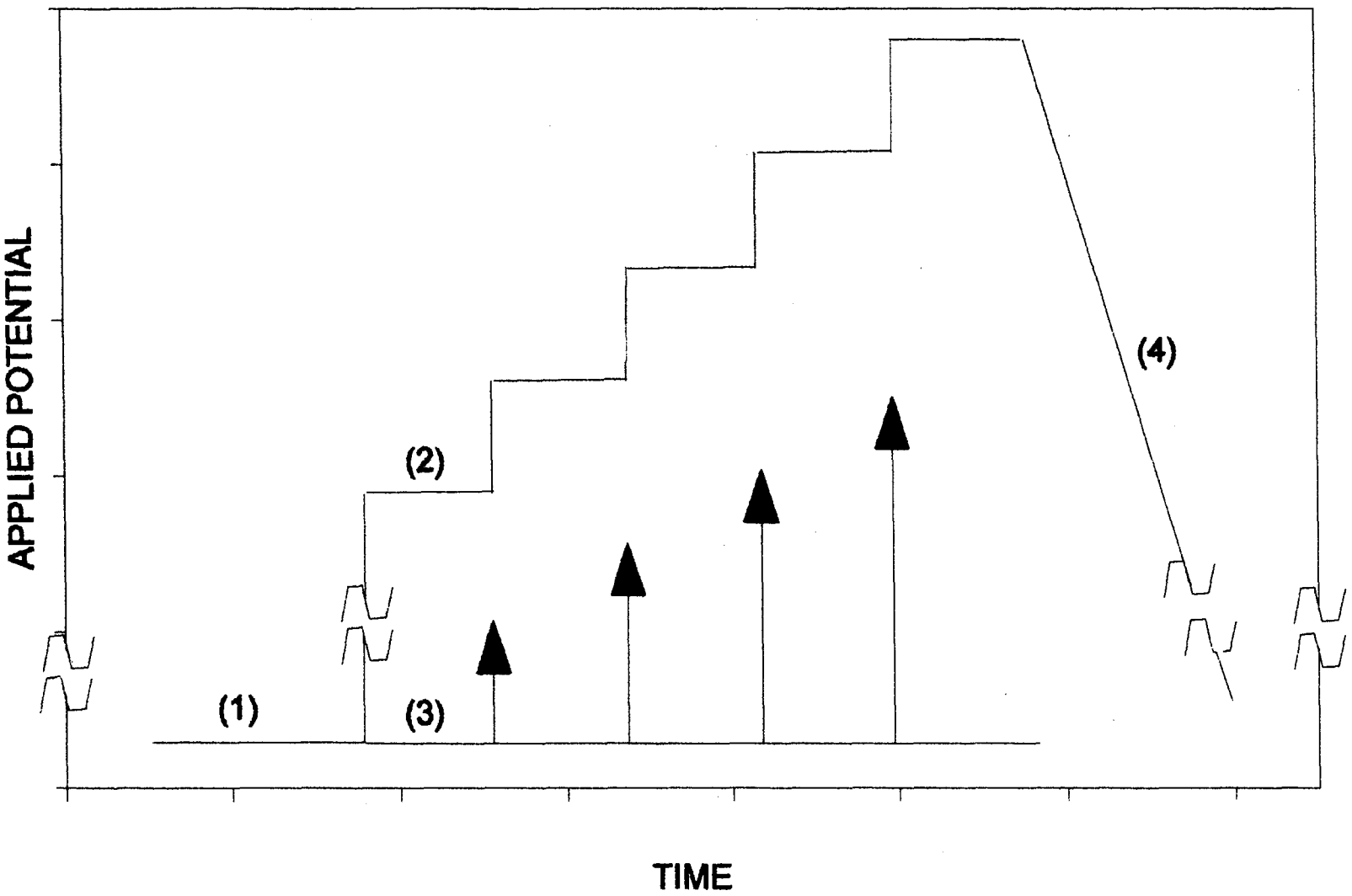

FIGURE 1: Schematic Showing the Potential-time Profiles Used to Obtain Anodic Dissolution Currents for UO_2: (1) Potential at Which the Electrode Was Prereduced (-2.0 V); (2) Anodic Dissolution Current Recorded at a Sequence of Consecutive Potentials; (3) Anodic Dissolution Current Recorded at Individual Potentials with Repreparation of the Electrode in Between; (4) Voltammetric Scan to -2.0 V at 20 mV $\cdot s^{-1}$ after Recording Anodic Currents by Either Procedure 1 or 2

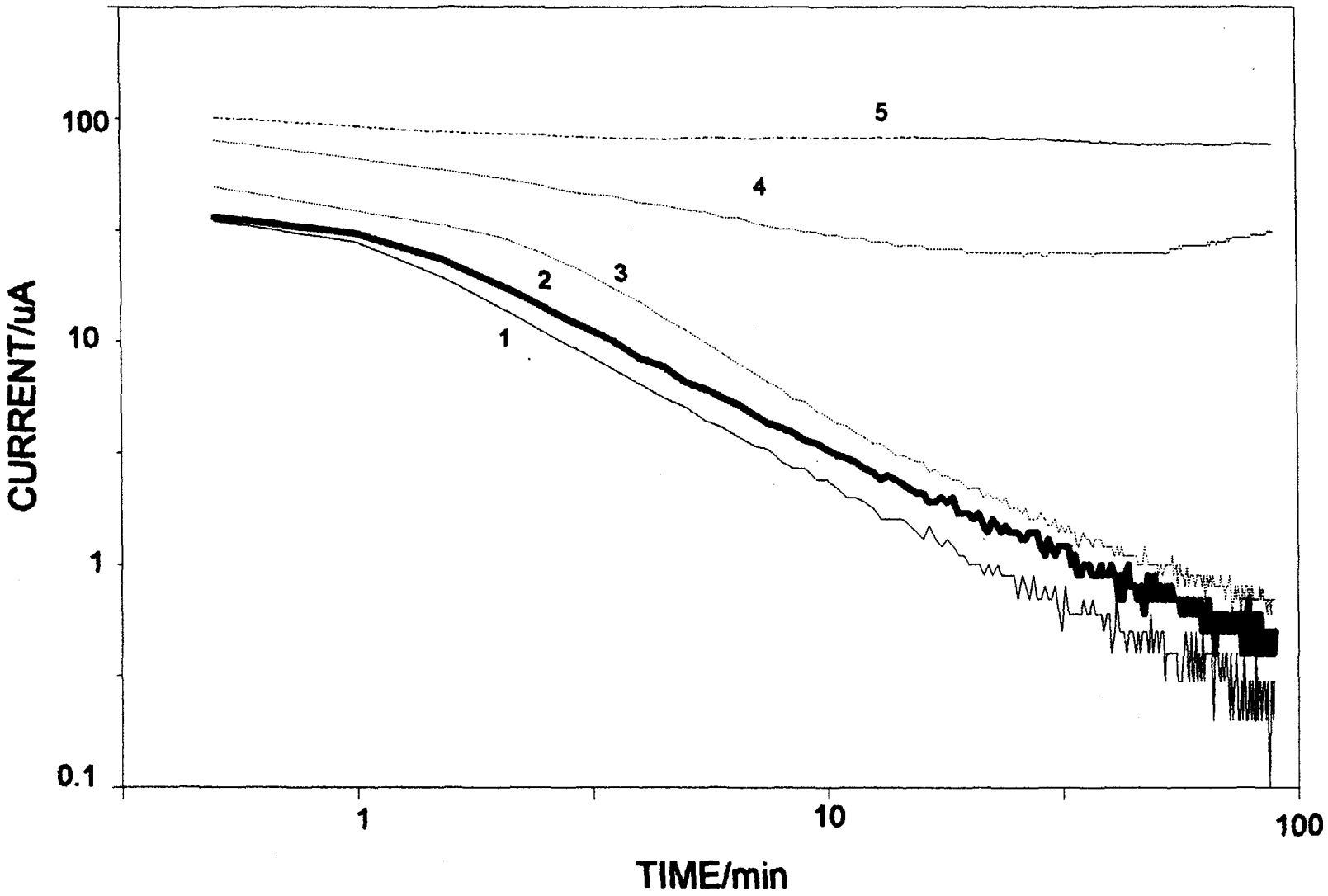

FIGURE 2: Logarithmic Current-Time Plots Recorded Individually (by Procedure 3, Figure 1) at a Series of Potentials by Pulsing Directly from -2.0 V Without Preoxidation at 0.1 V in 0.1 mol·L^{-1} $NaClO_4$ (pH = 9.5); ω = 16.7 Hz: (1) 0.175 V; (2) 0.275 V; (3) 0.325 V; (4) 0.375 V; (5) 0.400 V

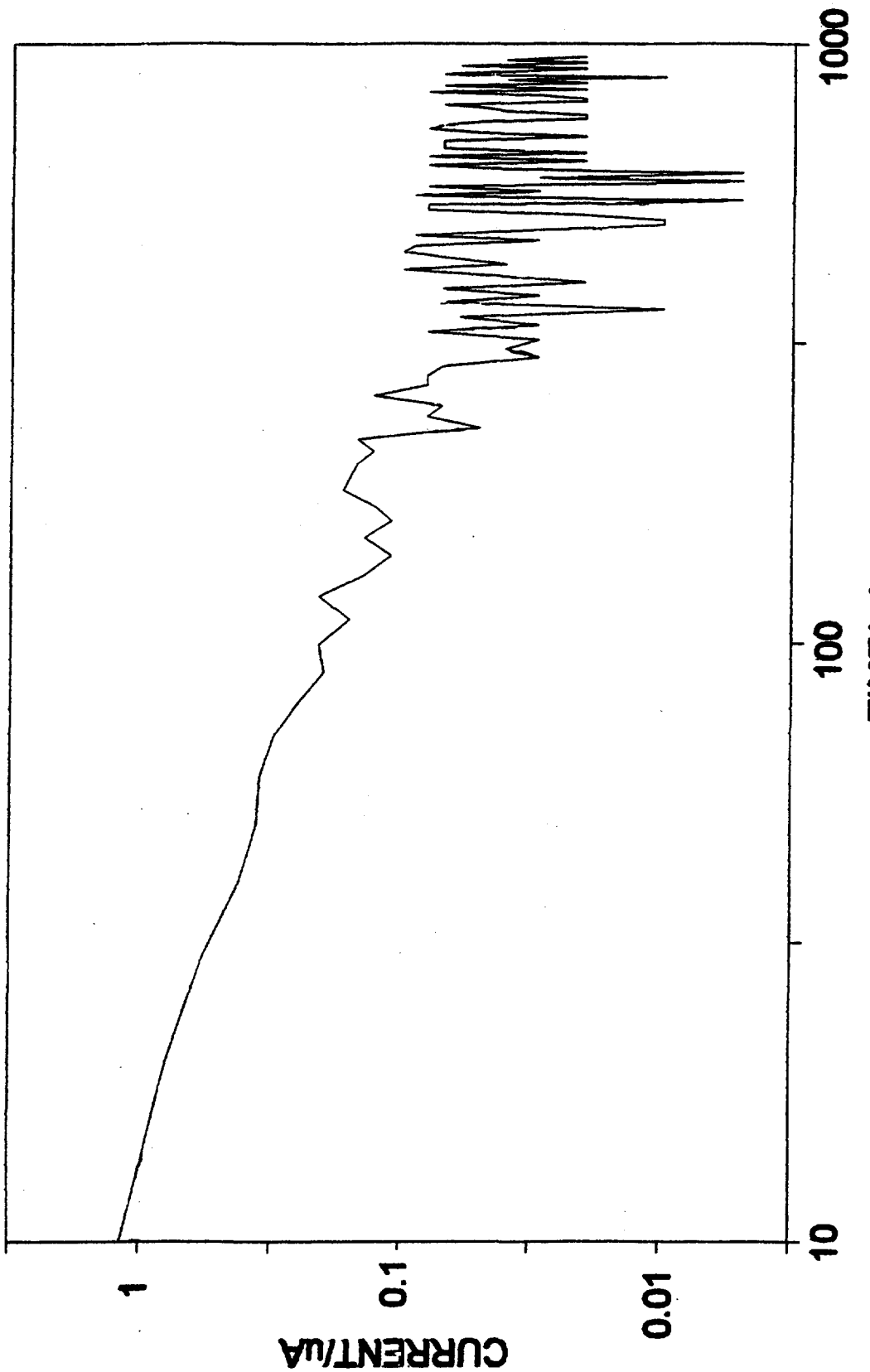

FIGURE 3: Logarithmic Current-time Plot Recorded at +0.100 V in 0.1 mol·L^{-1} $NaClO_4$ pH = 9.5; ω = 16.7 Hz

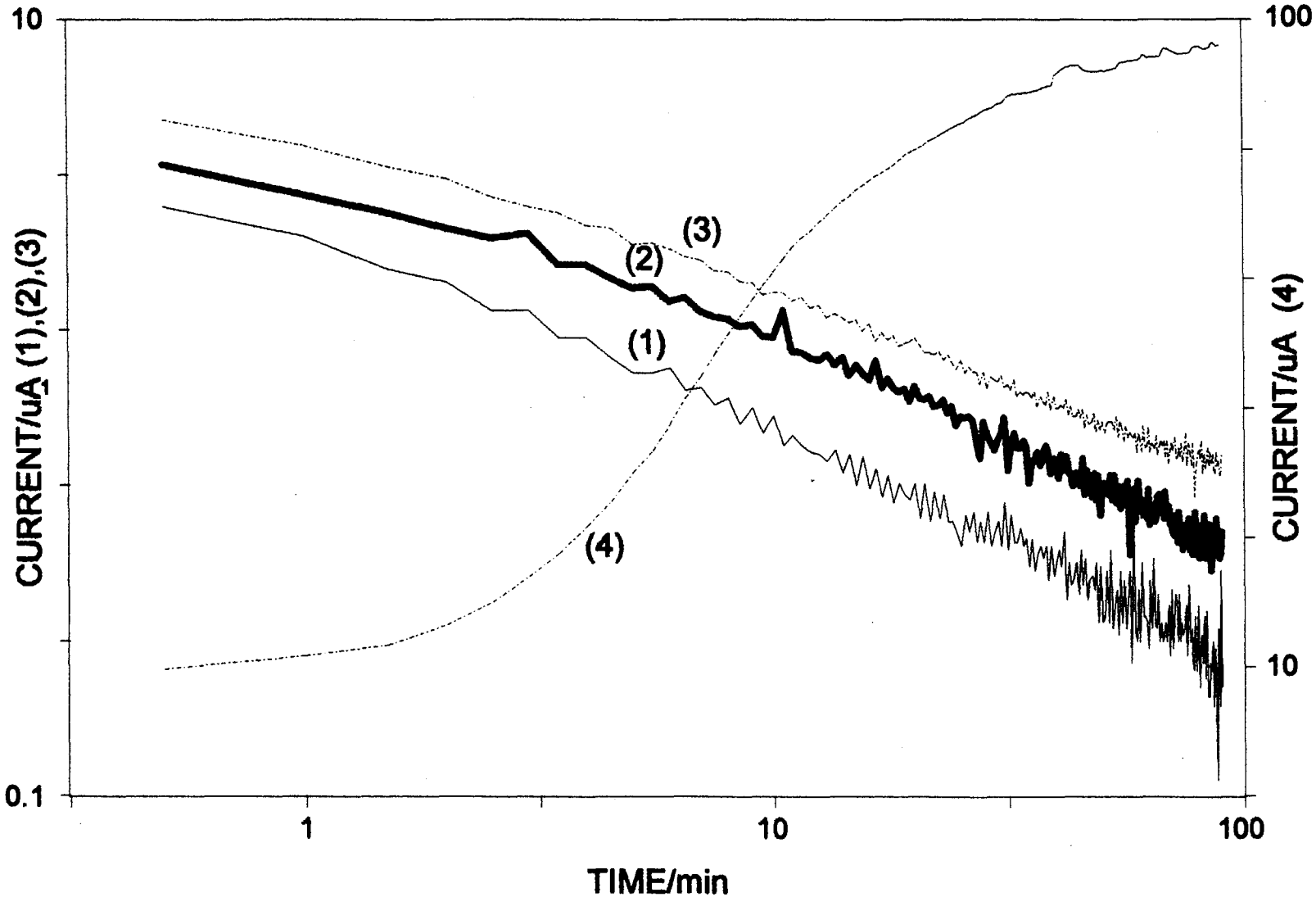

FIGURE 4: Logarithmic Current-time Plots Recorded Consecutively (by Procedure 2, Figure 1) at a Sequence of Potentials after Preoxidation at 0.100 V for ~24 h in 0.1 mol·L^{-1} $NaClO_4$ (pH = 9.5) ω = 16.7 Hz: (1) 0.150 V; (2) 0.250 V; (3) 0.350 V; (4) 0.450 V

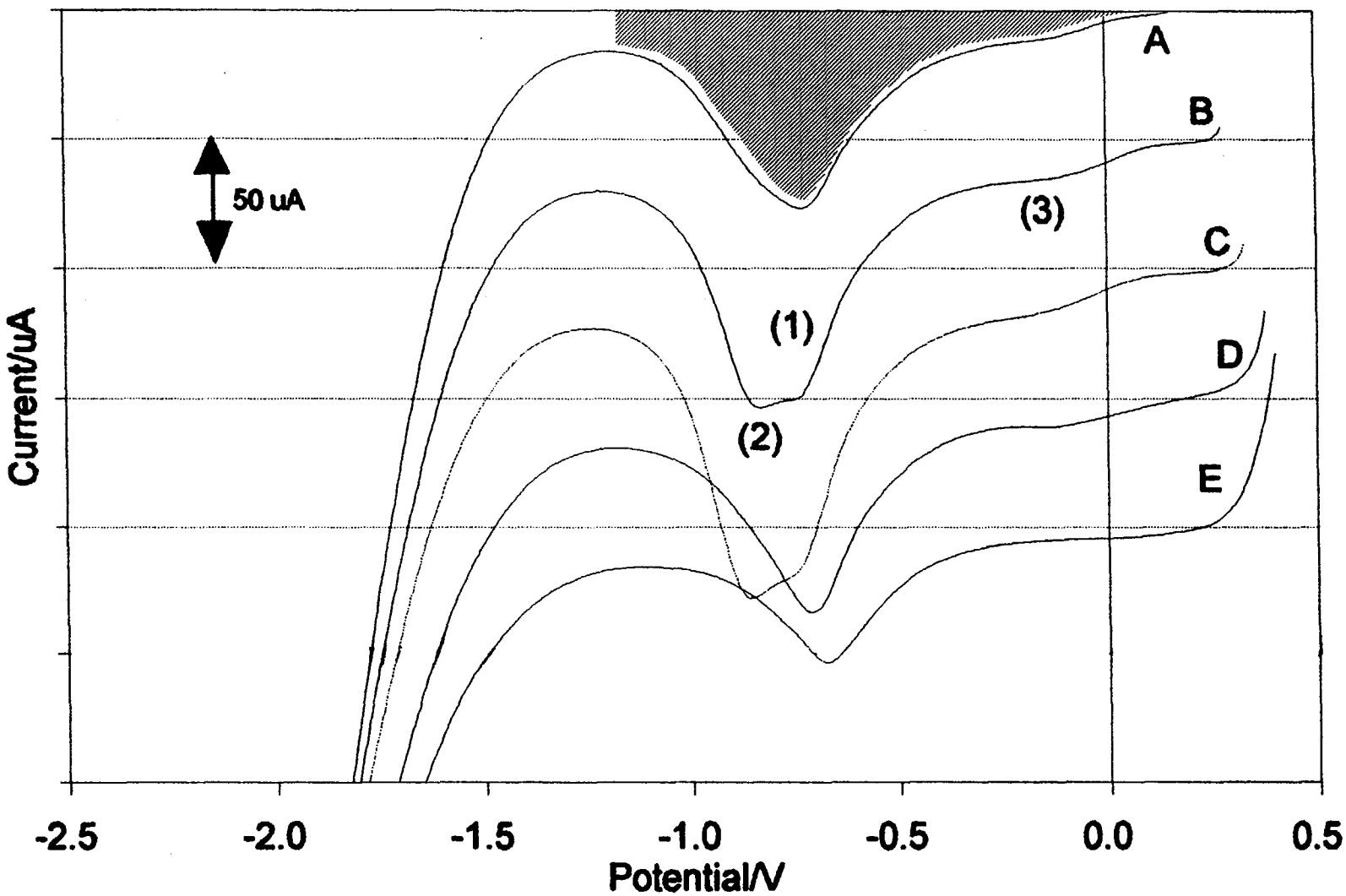

FIGURE 5: Cathodic Stripping Voltammograms (CSV) Recorded at Each Potential After Completing the Anodic Oxidations Described in Figure 2: (A) 0.175 V; (B) 0.275 V; (C) 0.325 V; (D) 0.375 V; (E) 0.400 V. The curves are vertically offset by 50 μA.

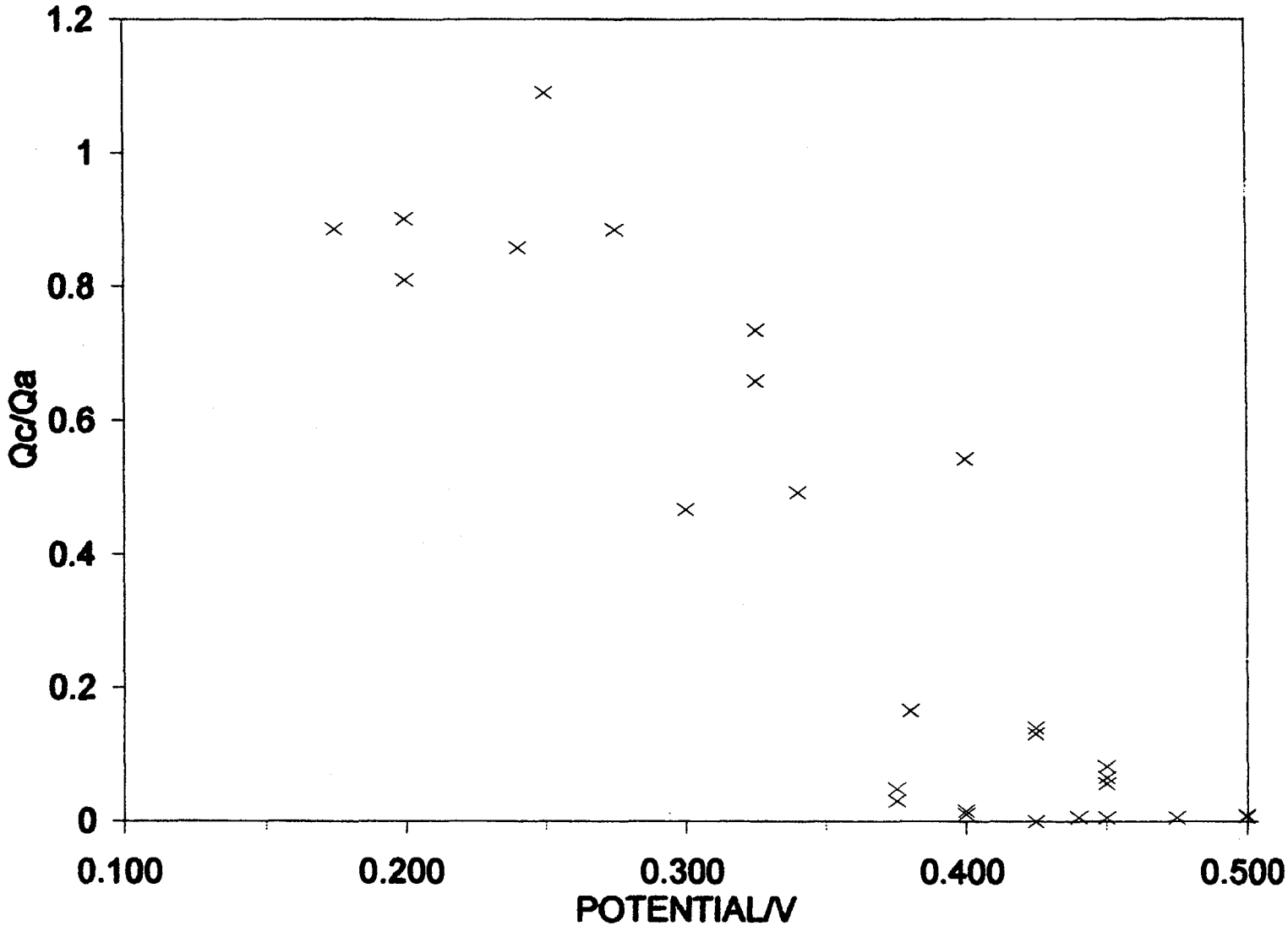

FIGURE 6: The Charge Ratio Q_C/Q_A, as a Function of Applied Anodic Potential (E_A). Q_A values were obtained from experiments in which the anodic oxidation was performed potentiostatically at a single potential. Q_C values were obtained from CSVs.

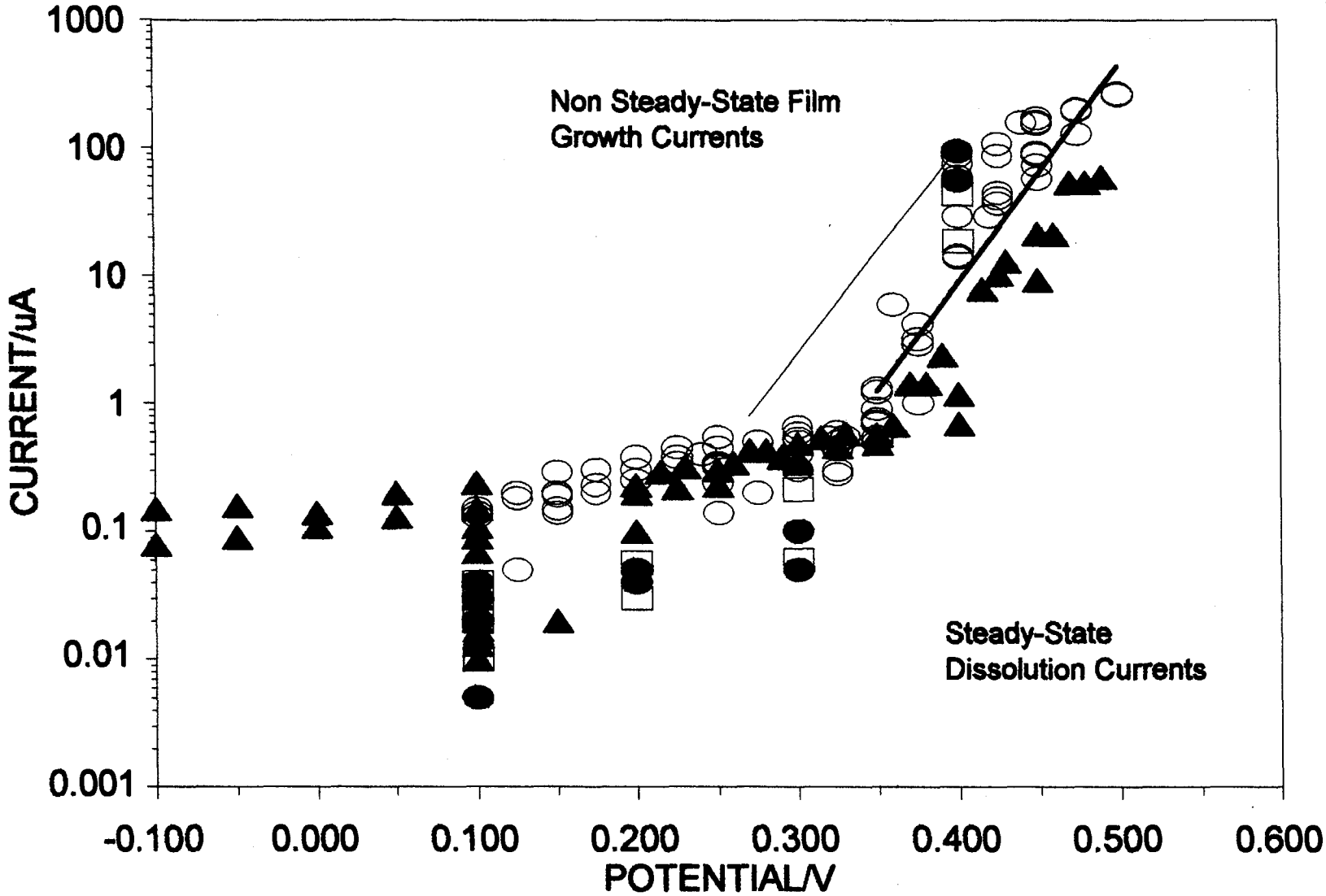

FIGURE 7: Logarithmic Current (i)-Potential (E) Plots Recorded on Rotating Disc Electrodes Cut from Different UO_2 Pellets in 0.1 mol·L^{-1} $NaClO_4$ (pH = 9.5), ω = 16.7 Hz: (▲) Currents Recorded on Electrode L; (o) Currents Recorded on Electrode R; (□) Currents Recorded on Electrode L after 14 to 20 h of Oxidation at Each Potential; (•) Current Recorded on Electrode R after 26 h of Oxidation. (—) linear fit to the points for E > 0.300 V; (——) linear fit from previously published data [29].

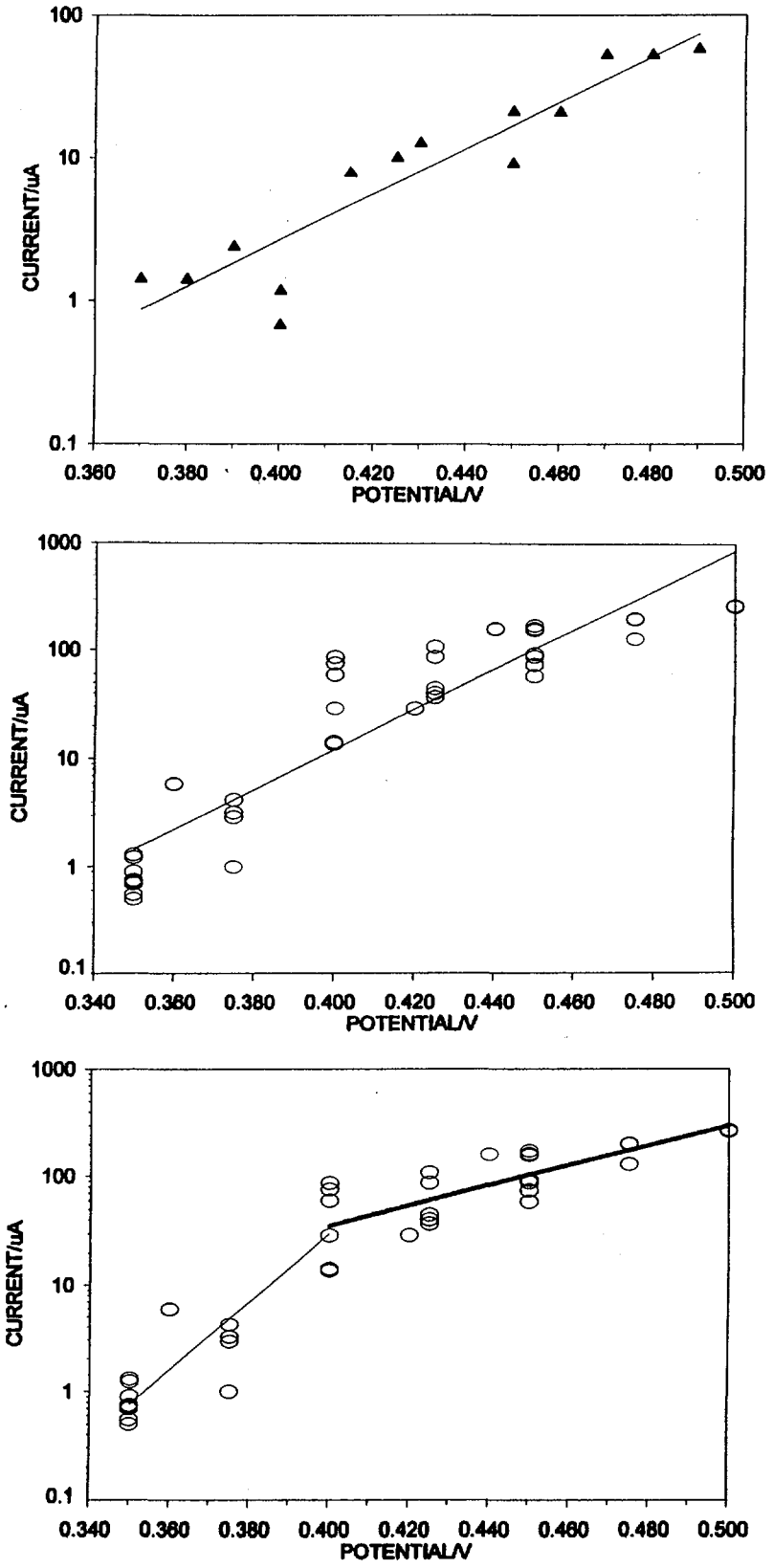

FIGURE 8: Tafel Plots for the Data Recorded at E > 0.300 V for Electrodes L and R (from Figure 7): (A) Electrode L; (B) Electrode R; (C) Electrode R Assuming Two Distinct Linear Regions (0.350 V ≤ E ≤ 0.400 V and 0.400 V ≤ E ≤ 0.550 V

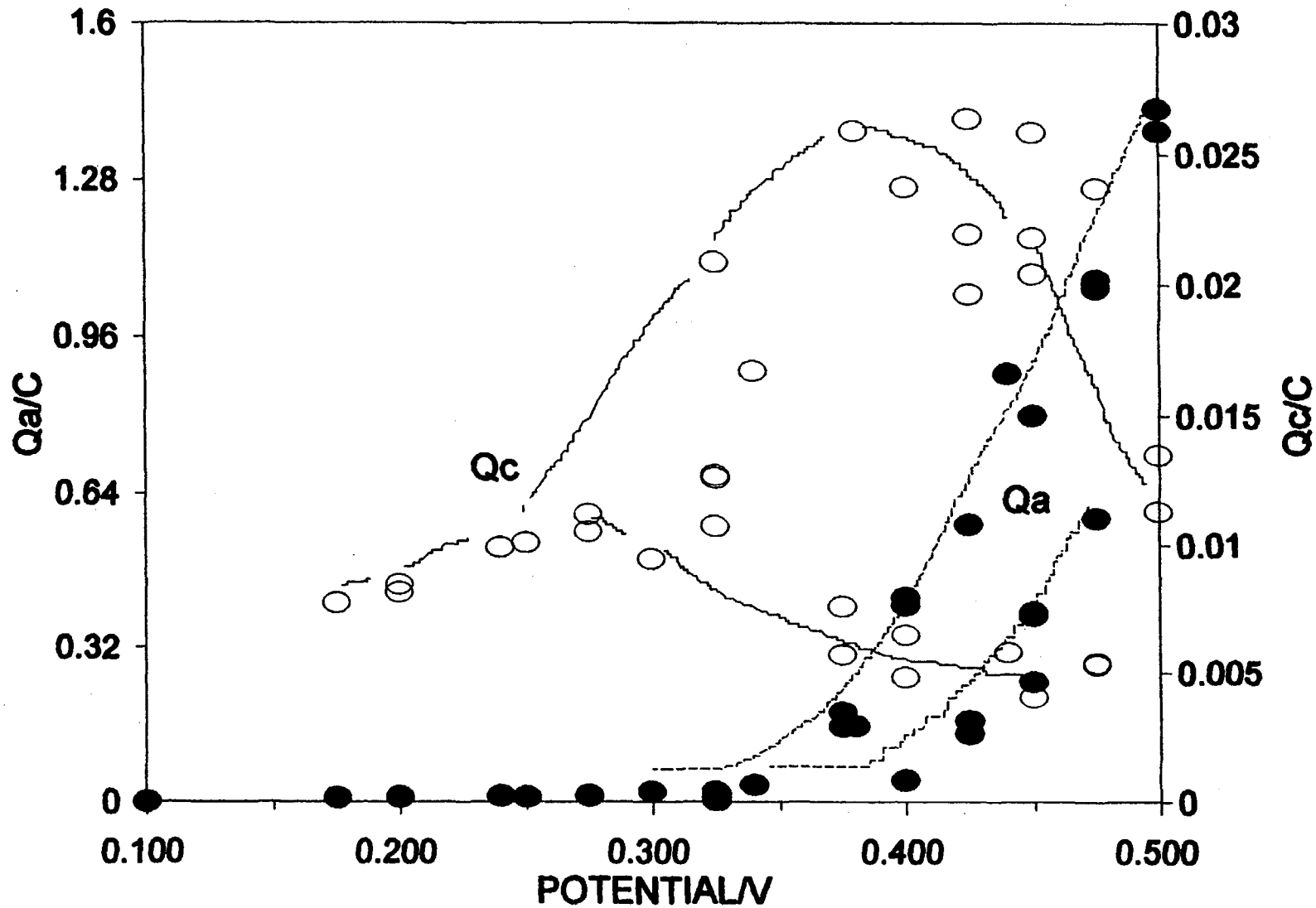

FIGURE 9: Q_A (•), Q_C(○) Values as a Function of the Single Applied Potential at Which the Anodic Oxidation Was Performed (i.e., Procedure 3, Figure 1). Values of Q_A obtained from integrated i-t plots: values of Q_C from CSVs.

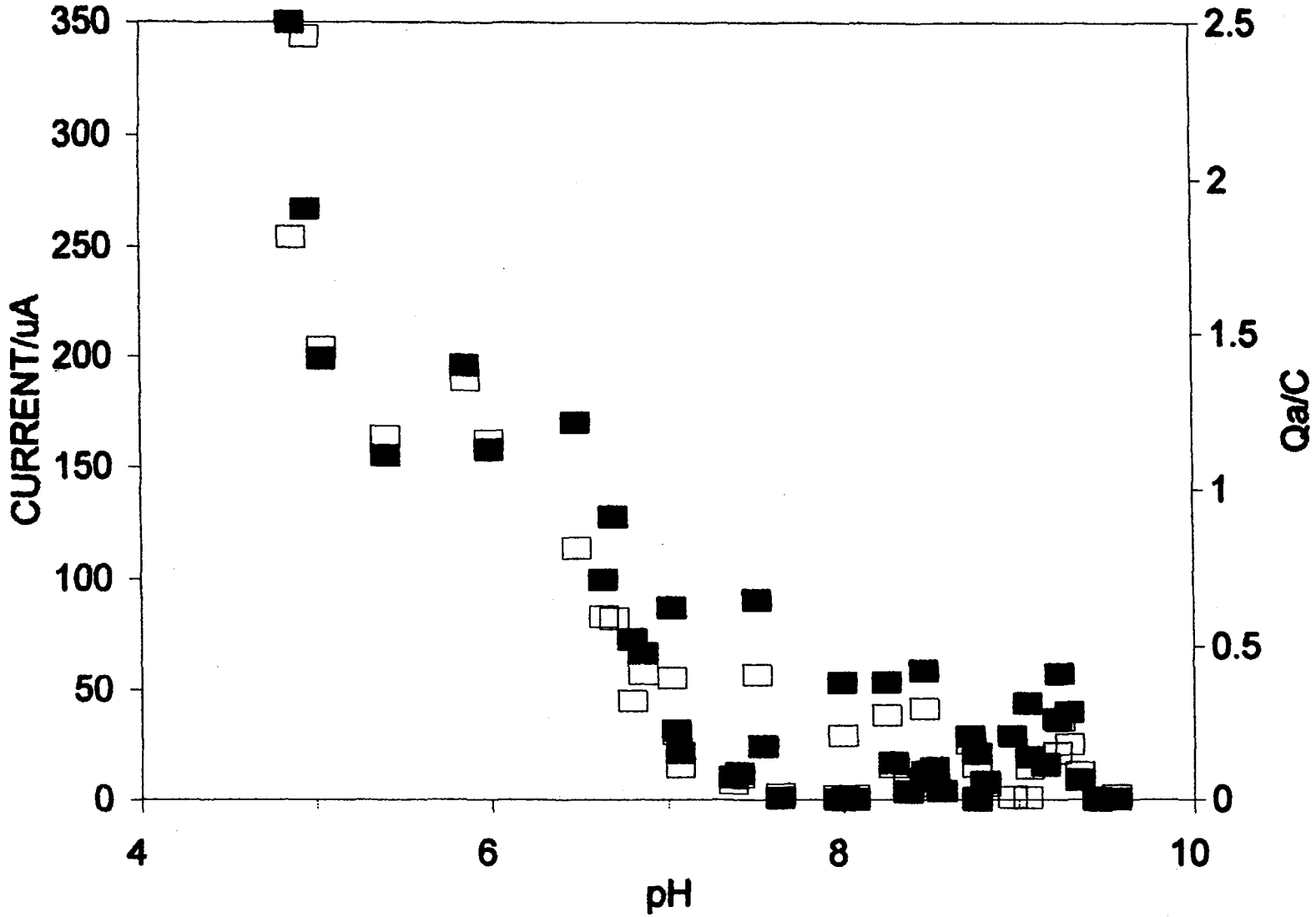

FIGURE 10: Plot of the Steady-State Currents (i_{ss} ,■, and Anodic Charges (Q_A), □, as a Function of the Final pH of the Bulk Solution for Anodic Oxidation at $E \geq 0.350$ V

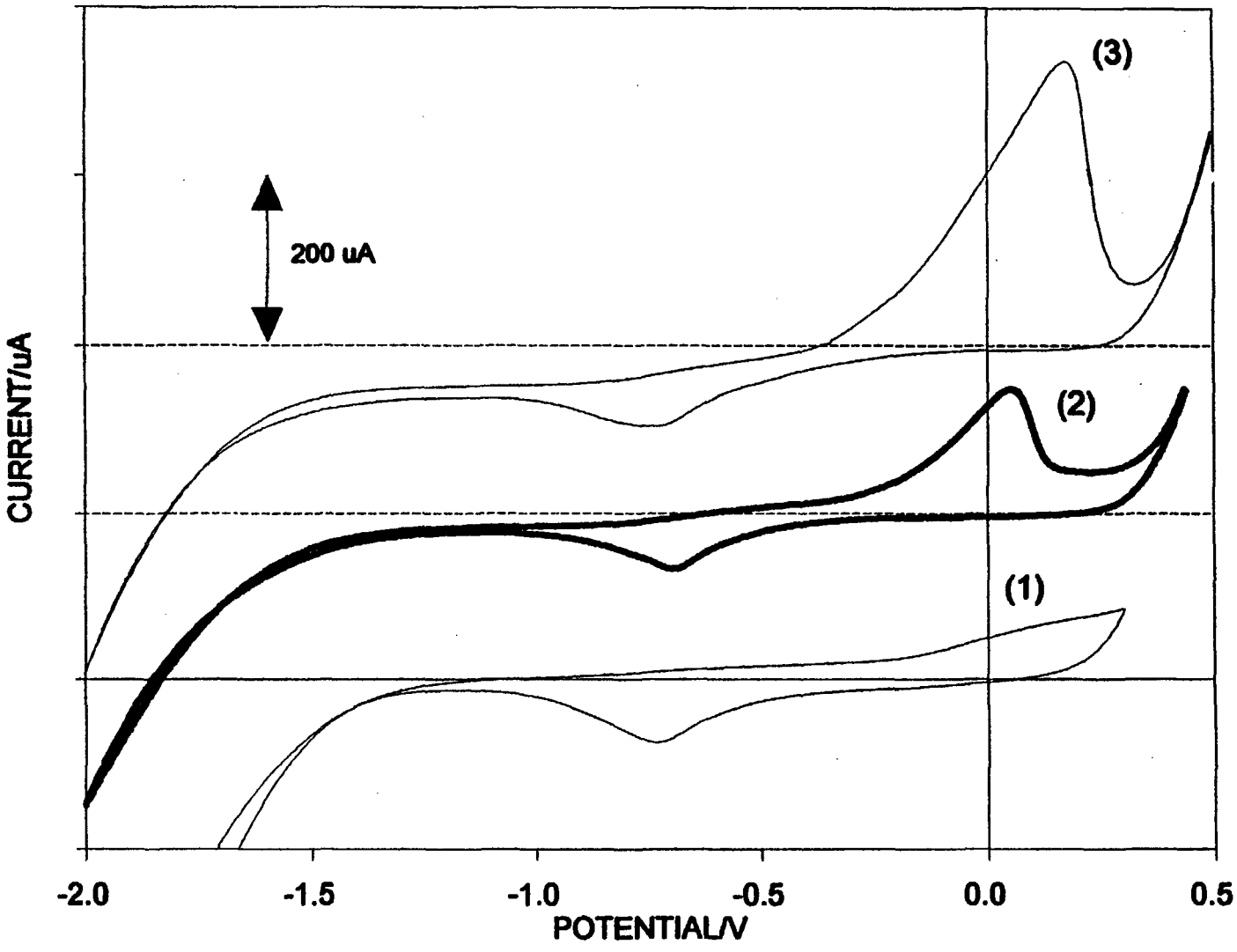

FIGURE 11: Cyclic Voltammograms Recorded on Electrode R in 0.1 mol·L^{-1} $NaClO_4$ (pH = 9.5), ω = 16.7 Hz: (1) Recorded on a Freshly Polished Electrode after Cathodic Reduction at -2.0 V; (2) Recorded after Preoxidation at 0.100 V (16 h) Followed by Oxidation at a Sequence of Potentials (1.5 h Each) up to 0.440 V (i_{ss} = 158 µA, Q_A = 211 mC); (3) Recorded after Preoxidation at +0.100 V (16 h) Followed by Oxidation at a Sequence of Potentials (1.5 h) up to 0.500 V (i_{ss} = 261 µA, Q_A = 2550 mC

Cat. No. / N° de cat.: CC2-11440E
ISBN 0-660-16454-X
ISSN 0067-0367

To identify individual documents in the series, we have assigned an AECL- number to each. Please refer to the AECL- number when requesting additional copies of this document from

Scientific Document Distribution Office (SDDO)
AECL
Chalk River, Ontario
Canada K0J 1J0

Fax: (613) 584-1745 Tel.: (613) 584-3311
ext. 4623

Price: A

Pour identifier les rapports individuels faisant partie de cette série, nous avons affecté un numéro AECL- à chacun d'eux. Veuillez indiquer le numéro AECL- lorsque vous demandez d'autres exemplaires de ce rapport au

Service de Distribution des documents officiels (SDDO)
EACL
Chalk River (Ontario)
Canada K0J 1J0

Fax: (613) 584-1745 Tél.: (613) 584-3311
poste 4623

Prix: A